



Geophysical Research Letters

RESEARCH LETTER

10.1002/2014GL061414

Key Points:

- Magnetosonic waves are excited by ion ring distributions near the plasmapause
- Magnetosonic waves are trapped in a limited radial region in the plasmasphere
- Magnetosonic waves are modulated by local density structures

Correspondence to:

Q. Ma,
qianlima@atmos.ucla.edu

Citation:

Ma, Q., W. Li, L. Chen, R. M. Thorne, C. A. Kletzing, W. S. Kurth, G. B. Hospodarsky, G. D. Reeves, M. G. Henderson, and H. E. Spence (2014), The trapping of equatorial magnetosonic waves in the Earth's outer plasmasphere, *Geophys. Res. Lett.*, 41, 6307–6313, doi:10.1002/2014GL061414.

Received 1 AUG 2014

Accepted 5 SEP 2014

Accepted article online 8 SEP 2014

Published online 23 SEP 2014

The trapping of equatorial magnetosonic waves in the Earth's outer plasmasphere

Q. Ma¹, W. Li¹, L. Chen², R. M. Thorne¹, C. A. Kletzing³, W. S. Kurth³, G. B. Hospodarsky³, G. D. Reeves⁴, M. G. Henderson⁴, and H. E. Spence⁵

¹Department of Atmospheric and Oceanic Sciences, University of California, Los Angeles, California, USA, ²Physics Department, W. B. Hanson Center for Space Sciences, University of Texas at Dallas, Richardson, Texas, USA, ³Department of Physics and Astronomy, University of Iowa, Iowa City, Iowa, USA, ⁴Space Science and Applications Group, Los Alamos National Laboratory, Los Alamos, New Mexico, USA, ⁵Institute for the Study of Earth, Oceans, and Space, University of New Hampshire, Durham, New Hampshire, USA

Abstract We investigate the excitation and propagation of equatorial magnetosonic waves observed by the Van Allen Probes and describe evidence for a trapping mechanism for magnetosonic waves in the Earth's plasmasphere. Intense equatorial magnetosonic waves were observed inside the plasmasphere in association with a pronounced proton ring distribution, which provides free energy for wave excitation. Instability analysis along the inbound orbit demonstrates that broadband magnetosonic waves can be excited over a localized spatial region near the plasmapause. The waves can subsequently propagate into the inner plasmasphere and remain trapped over a limited radial extent, consistent with the predictions of near-perpendicular propagation. By performing a similar analysis on another observed magnetosonic wave event, we demonstrate that magnetosonic waves can also be trapped within local density structures. We suggest that perpendicular wave propagation is important for explaining the presence of magnetosonic waves in the Earth's plasmasphere at locations away from the generation region.

1. Introduction

Equatorial magnetosonic waves are oblique whistler mode electromagnetic emissions between the proton gyrofrequency and the lower hybrid resonant frequency [Perraut *et al.*, 1982; Laakso *et al.*, 1990; Santolík *et al.*, 2004], observed near the Earth's magnetic equator [Russell and Holzer, 1970; Gurnett, 1976; Santolík *et al.*, 2002], and may have potentially important effects in particle scattering in the radiation belts [Horne *et al.*, 2007; Bortnik and Thorne, 2010; Mourenas *et al.*, 2013; Xiao *et al.*, 2014]. Recent spacecraft missions in the Earth's magnetosphere have provided excellent coverage for investigating magnetosonic wave spectral properties, spatial distributions, and their dependences on the local plasma conditions [Santolík *et al.*, 2004; Meredith *et al.*, 2008; Ma *et al.*, 2013]. Magnetosonic waves in the Earth's inner magnetosphere are excited by positive phase space density (PSD) slopes in the ion ring distribution over the energy range from ~ 1 keV to ~ 30 keV [Perraut *et al.*, 1982; Horne *et al.*, 2000; Thomsen *et al.*, 2011; Chen *et al.*, 2011; Liu *et al.*, 2011; Xiao *et al.*, 2013], and the unstable frequency spectra and local wave growth rates are modulated by the relative ratio between the local Alfvén energy (E_A) and ion ring energy (E_R) [Boardsen *et al.*, 1992; Chen *et al.*, 2010].

The global surveys of magnetosonic waves have shown that magnetosonic waves have higher occurrence rates outside the plasmapause than inside the plasmapause, due to their strong dependence on the presence of ion ring distributions [Meredith *et al.*, 2008; Ma *et al.*, 2013]. With simultaneous observations of ion ring distributions with E_R close to E_A , magnetosonic waves outside the plasmapause can generally be explained by a local excitation mechanism [e.g., Ma *et al.*, 2014]. However, the local excitation mechanism cannot explain the presence of magnetosonic waves deep inside the plasmapause where E_A becomes much less than E_R , and the conditions for local generation of magnetosonic waves are typically not satisfied [Chen *et al.*, 2010; Ma *et al.*, 2014]. Nonetheless, magnetosonic waves are observed over a wide range of L shells inside the plasmasphere, and their distributions are more uniform inside the plasmapause than outside the plasmapause [Meredith *et al.*, 2008; Ma *et al.*, 2013]. Observational evidence indicates that magnetosonic waves can propagate both radially and azimuthally [Santolík *et al.*, 2002], and the analysis by Chen and Thorne [2012] has shown that magnetosonic waves within a wide range of azimuthally propagating angles may become trapped between the outer edge of the plasmapause and deep in the plasmasphere. Consequently,

it is necessary to incorporate propagation effects together with the local excitation mechanism to reconstruct the observed magnetosonic wave events inside the plasmapause.

Using the Van Allen Probes wave and particle measurements, we perform a combined wave excitation and propagation analysis on two magnetosonic wave events and directly demonstrate that magnetosonic waves can be excited near the plasmapause and subsequently be trapped inside the plasmasphere or within local density structures. Our study indicates the importance of wave propagation in understanding the magnetosonic wave distribution in the plasmasphere.

2. Magnetosonic Wave Instability Analysis and Trapping in the Plasmasphere

The Van Allen Probes are two identical spacecraft (Probes A and B) in nearly equatorial orbits with a perigee $\sim 1.1 R_E$ and an apogee $\sim 5.9 R_E$ [Mauk et al., 2012] and provide high-resolution particle and wave measurements in the Earth's inner magnetosphere. The Energetic Particle Composition and Thermal Plasma Suite (ECT) [Spence et al., 2013] measures the radiation belt electron and ion spectra with sufficient energy and pitch angle coverage, and the Helium, Oxygen, Proton, and Electron (HOPE) instrument [Funsten et al., 2013] covers the particle energy range from ~ 1 eV to ~ 50 keV. The Electric and Magnetic Field Instrument Suite and Integrated Science (EMFISIS) [Kletzing et al., 2013] measures the DC magnetic field (Magnetometer) and the wave electric and magnetic fields (Waves instrument). The Waveform Receiver (WFR) of the Waves instrument measures wave spectra from 10 Hz to 12 kHz for the three components of both electric field and magnetic field. The WFR not only measures wave power spectral density but also provides wave polarization properties including wave normal angle, azimuthal angle, and ellipticity, calculated by the Singular Value Decomposition method [Santolík et al., 2003]. The High-Frequency Receiver (HFR) of the Waves instrument measures the electric field spectra density from 10 kHz to 400 kHz [Kletzing et al., 2013], which covers the upper hybrid resonance frequency f_{UHR} and can therefore be used to infer the plasma density in the Earth's radiation belts.

Figure 1 presents the intense magnetosonic wave and ion ring event observed by Van Allen Probe A during 0930–1200 UT on 4 December 2012. The spacecraft was traveling nearly radially inward near the Earth's magnetic equator. The upper hybrid resonance frequency line (the white solid line) in the HFR spectra (Figure 1a) indicates that the spacecraft was inside the plasmapause after ~ 0950 UT. The proton phase space density (PSD) measurements at different energies and pitch angles (not explicitly shown here) indicate the existence of the ion ring distribution. The energy spectra of proton PSD at a pitch angle of 90° (Figure 1b) show that an ion ring distribution was formed inside the plasmapause and extended deep into the plasmasphere. The proton ring energy E_R , which is defined as the proton perpendicular energy associated with the peak PSD value, is a few keV. Previous analysis [Chen et al., 2010, 2011] has demonstrated that an ion ring distribution may potentially excite magnetosonic waves when E_R is close to the local Alfvén energy E_A ($E_A = B_0^2/(2\mu_0 N)$, where μ_0 is the vacuum permeability, N is the plasma density, and B_0 is the background magnetic field intensity). Magnetosonic waves below the lower hybrid resonance frequency f_{LHR} (the white solid line) are captured in the WFR magnetic field power spectrogram (Figure 1c). Between ~ 1008 UT and ~ 1115 UT, the magnetosonic waves have nearly constant frequencies, become most intense at around 1020 UT, and gradually fade farther inside the plasmasphere. After ~ 1115 UT, the spacecraft observed weaker magnetosonic waves extending to increasingly higher frequencies, following the f_{LHR} trend. We integrated the magnetic field power spectral density over the frequencies between f_{cp} and f_{LHR} to obtain the wave amplitude during the magnetosonic wave event. The magnetosonic wave amplitude (Figure 1d) remained higher than 100 pT for ~ 15 min, indicating that strong magnetosonic waves were present over a broad region near the equatorial plane. The wave normal angle distribution (Figure 1e) shows that the waves are highly oblique; thus, the wave vectors lie near the equatorial plane, and the waves can propagate both radially and azimuthally. The high wave magnetic compressibility (Figure 1f) indicates that the wave magnetic component parallel to the background magnetic field is the dominant component, and these waves are fast magnetosonic mode.

Using the same technique as Ma et al. [2014], we perform a local magnetosonic wave instability analysis on the observed proton PSD distribution with full pitch angle coverage obtained from the HOPE instrument. The wave growth rates (Figure 1g) are calculated from ~ 1008 UT to 1200 UT when the ion ring distributions are present, and the results are clearly modulated by the relative ratio of E_A (the white solid line in Figure 1b) to E_R (the black dotted line in Figure 1b). Close to the plasmapause, E_A is slightly lower than E_R , and strong

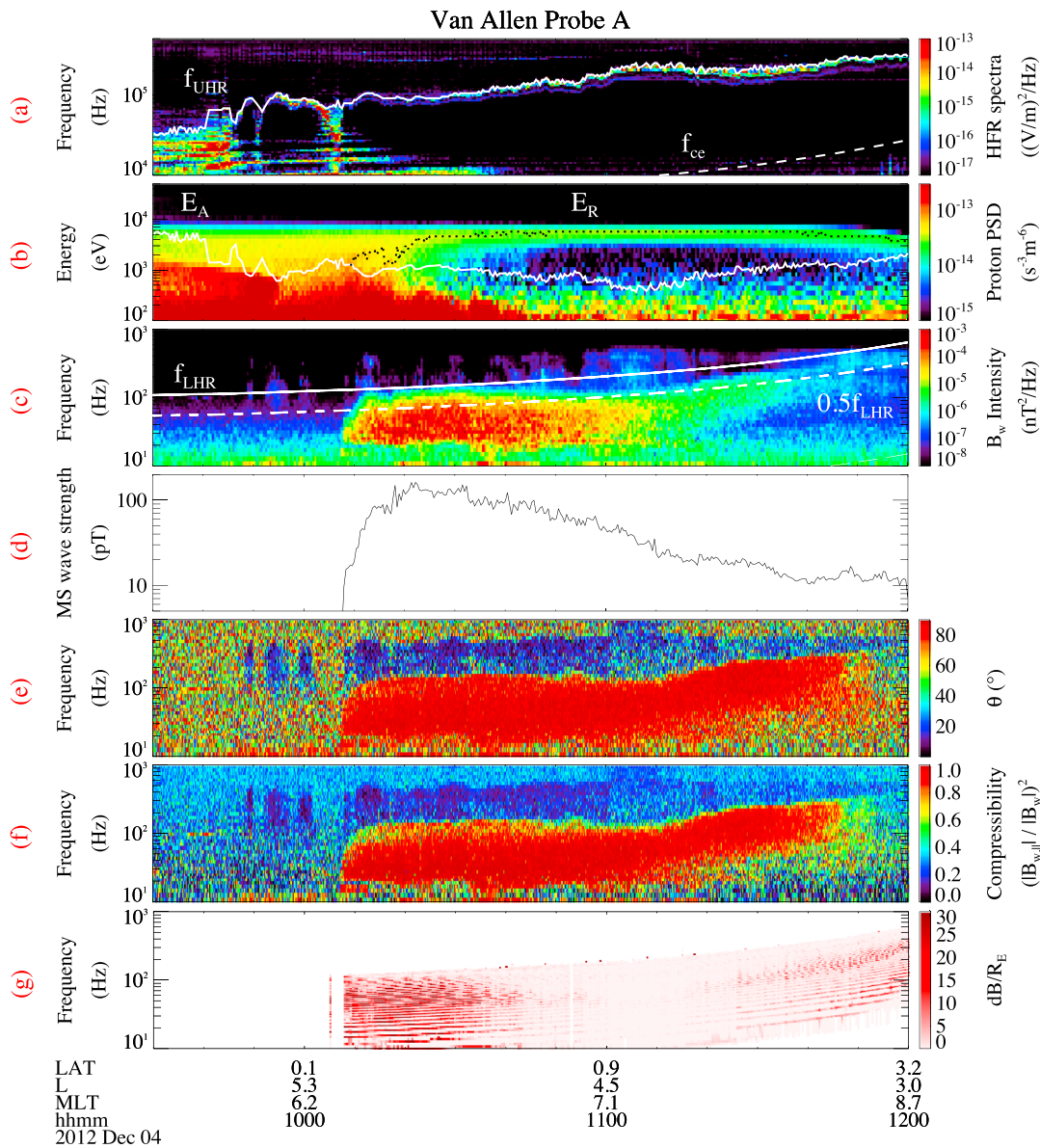


Figure 1. Magnetosonic waves observed by Van Allen Probe A on 4 December 2012 and the instability analysis. (a) The electric field power spectral density in the Waves HFR channel; (b) proton PSD as a function of energy for a pitch angle of $\sim 90^\circ$ measured by the HOPE instrument; (c) magnetic field power spectral density in the Waves WFR channel; (d) magnetic wave amplitudes of magnetosonic waves; (e) magnetosonic wave normal angles; (f) wave magnetic compressibility ($|B_{w\parallel}|/|B_w|^2$, where $B_{w\parallel}$ and B_w are the parallel component of the wave magnetic field power spectral density and the total wave magnetic field power spectral density, respectively); (g) calculated magnetosonic wave local growth rates. In Figure 1a, the white solid line and the white dashed line represent f_{UHR} and the equatorial electron cyclotron frequency f_{ce} , respectively; In Figure 1b, the white solid line and the black dotted line represent the Alfvén energy E_A and the ion ring energy E_R , respectively; In Figure 1c, the white solid line and the white dashed line represent f_{LHR} and $0.5 f_{LHR}$, respectively.

growth rates occur over a broad frequency band. The local growth rates fade away after ~ 1040 UT when the ratio of E_A/E_R drops below ~ 0.1 . Deeper inside the plasmasphere after ~ 1130 UT, E_A gradually increases to become slightly lower than E_R , and the calculation of magnetosonic wave growth rate exhibits modestly positive values associated with the weak proton ring distributions. The local instability analysis is consistent with the observed magnetosonic wave power spectrum in the outer region before ~ 1040 UT but cannot account for the existence of relatively strong magnetosonic waves between 1045 UT and 1115 UT.

According to the magnetosonic wave propagation analysis in *Chen and Thorne [2012]*, the quantity $Q = nL \sin(\varphi)$ is conserved along the raypath during near-perpendicular propagation in an axisymmetric or locally axisymmetric medium, where n is the refractive index and φ is the wave azimuthal angle with 0° (180°) being

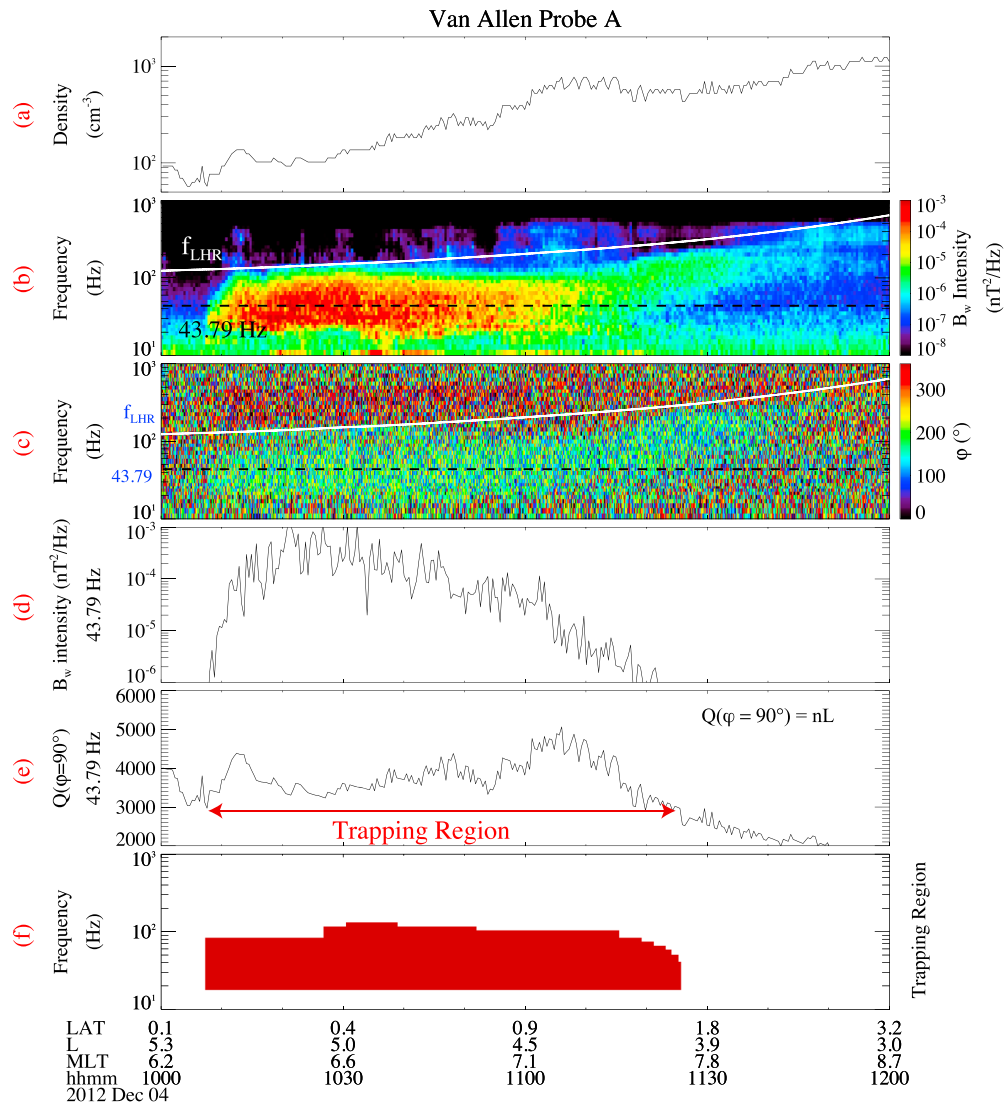


Figure 2. Trapping region analysis of magnetosonic wave event on 4 December 2012. (a) The total plasma density inferred from the upper hybrid resonance frequency line in Figure 1a; (b) magnetic field power spectral density in the Waves WFR channel; (c) azimuthal propagation angle; (d) wave magnetic field power spectral density at 43.79 Hz; (e) calculated Q ($\varphi = 90^\circ$) = nL profile at 43.79 Hz; (f) estimated magnetosonic wave trapping region. In Figures 2b and 2c, the white solid line and the black dashed line represent f_{LHR} and the frequency of 43.79 Hz, respectively; In Figure 2e, the red two-way arrow represents the predicted trapping region at 43.79 Hz.

directing radially outward (inward) and 90° (270°) being directing azimuthally toward later (earlier) local time. Consequently, magnetosonic waves launched over a wide range of azimuthal angles may be trapped in the outer plasmasphere due to the maximum of the refractive index at the inner edge of plasmapause for a given wave frequency. As wave propagates away from the inner edge, the refractive index decreases rapidly; thus, the azimuthal angle approaches 90° and radial reflection occurs. The ray can be reflected radially at the innermost or outermost L shell corresponding to the azimuthal angle of 90° . For a wave launched at given L, φ , and wave frequency, we can calculate corresponding Q and then determine the radial range of the innermost and outermost L shell of trapping region by the reflection condition $Q(\varphi = 90^\circ) = nL$ [Chen and Thorne, 2012]. We can use this range, which has wave frequency dependence, to predict the radial extent of magnetosonic wave trapping at different wave frequencies.

In Figure 2, we use the conservation of Q to study the effects of magnetosonic wave propagation during 1000–1200 UT on 4 December 2012. To analyze the trapping region of the observed magnetosonic wave

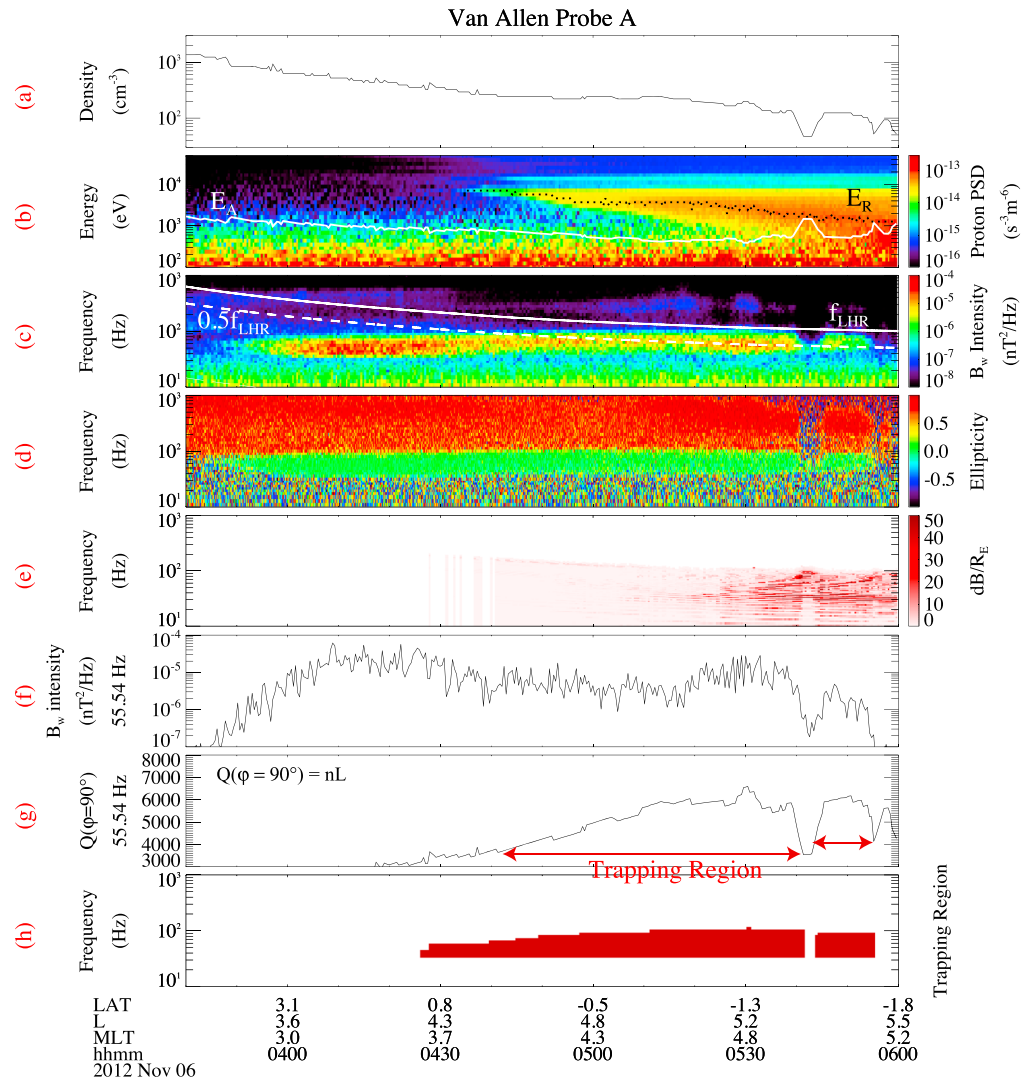


Figure 3. The local instability and trapping analysis of magnetosonic wave event on 6 November 2012. (a) The total plasma density inferred from the upper hybrid resonance frequency line measured by the Waves HFR channel; (b) proton PSD as a function of energy for a pitch angle of ~90° measured by the HOPE instrument; (c) magnetic field power spectral density in the Waves WFR channel; (d) wave ellipticity; (e) calculated magnetosonic wave local growth rates; (f) wave magnetic field power spectral density at 55.54 Hz; (g) calculated $Q(\varphi = 90^\circ) = nL$ profile at 55.54 Hz; (h) estimated magnetosonic wave trapping region. In Figure 3b, the white solid line and the black dotted line represent the Alfvén energy E_A and the ion ring energy E_R , respectively; In Figure 3c, the white solid line and the white dashed line represent f_{LHR} and $0.5 f_{LHR}$, respectively; In Figure 3g, the red two-way arrows represent the predicted trapping regions at 55.54 Hz.

event, we have made several assumptions: the magnetosonic waves propagate in a two-dimensional equatorial plane; the azimuthal spatial variations in the background plasma density are small; the temporal variations during the ~2 h period of the observation are small; the wave source is well captured by the spacecraft during its inbound or outbound orbit.

During the inbound path of the spacecraft, the plasma density (Figure 2a) increases from ~60 cm⁻³ at $L \sim 5.2$ to ~800 cm⁻³ at $L \sim 4.2$ where the magnetosonic waves fade out. The distribution of observed azimuthal wave angles (Figure 2c) is scattered, yet magnetosonic waves at the outer regions are observed to be mainly propagating inward to lower L shells. The magnetosonic wave intensity at 43.79 Hz is shown in Figure 2d, and we calculated the value of $Q(\varphi = 90^\circ) = nL$ at the same frequency in Figure 2e. After magnetosonic waves are locally excited inside $L \sim 5.2$, the outer boundary of the observed wave trapping (indicated by the left end of the red two-way arrow in Figure 2e) is used to identify the minimum $Q(\varphi = 90^\circ)$ value (Q_{min}), and the

inner boundary of the trapping region is then determined at the location where $Q(\varphi = 90^\circ)$ drops below Q_{\min} deep inside the plasmasphere (indicated by the right end of the red two-way arrow in Figure 2e). The predicted trapping region in Figure 2e agrees well with the observed wave intensity in Figure 2d. We also calculated the trapping region at different frequencies in Figure 2f. The simulated trapping region covers the observed wave extent reasonably well, indicating that magnetosonic waves are excited at relatively larger L shells mainly between ~ 5.0 and ~ 5.2 , subsequently are able to propagate inward to $L \sim 4.0$, and thus become trapped at L shells between ~ 4.0 and ~ 5.2 .

3. Magnetosonic Waves Trapped by Local Density Structures

Because the Q values are dependent on plasma density values, the local plasma density structures may produce a maximum of nL , therefore affecting the trapping regions and subsequently controlling the presence of trapped magnetosonic waves. Figure 3 shows an example of magnetosonic waves that are modulated by the local density structures in the plasmasphere. The density (Figure 3a) inferred from the wave power spectra in the HFR channel drops from more than 100 cm^{-3} to around 50 cm^{-3} at $L \sim 5.35$ and $L \sim 5.48$, respectively. The wave magnetic field power spectral intensity (Figure 3c) shows the intensification of magnetosonic waves with low ellipticity ~ 0 (Figure 3d), and the wave intensity modulation is associated with the density variations after ~ 0530 UT. The magnetosonic waves are also observed in a broad region inside the plasmasphere from ~ 0350 UT to 0540 UT. Clear ion ring distributions (Figure 3b) are observed after ~ 0440 UT, and the calculation of local magnetosonic wave growth rates (Figure 3e) shows that the ion rings can locally excite magnetosonic waves outside $L \sim 5.1$ where E_R (the black dotted line in Figure 3b) becomes comparable to E_A (the white solid line in Figure 3b).

We calculated the nL profile for 55.54 Hz in Figure 3g and the trapping region corresponding to each frequency band in Figure 3h. Our simulation of the trapping region clearly shows that the magnetosonic waves are trapped by the local density structure between $L \sim 5.35$ and $L \sim 5.48$, which agrees well with observations. Inside $L \sim 5.35$, magnetosonic waves can be trapped over a limited inward radial extent to $L \sim 4.2$ at a frequency of ~ 40 Hz, or to $L \sim 5.0$ at a frequency of ~ 100 Hz. However, magnetosonic waves are observed much farther inside the plasmasphere to $L \sim 3.35$. Also, the observed magnetosonic waves between $L \sim 3.7$ and $L \sim 4.2$ are much stronger than those in the identified source region outside $L \sim 5.1$. The observations are still consistent with our analysis provided that the magnetosonic waves inside $L \sim 4.2$ originate from another source that is not encountered by the localized trajectory of the Van Allen Probes.

4. Conclusions and Discussions

We have used the Van Allen Probes EMFISIS wave data and HOPE proton flux data to investigate the instability and trapping mechanisms of magnetosonic waves in the Earth's plasmasphere. The EMFISIS instrument suite provides continuous high-resolution equatorial magnetosonic wave measurements and essential information about the wave power spectrogram and polarization properties. The HOPE instrument provides high-resolution particle flux measurements which are needed for the analysis of magnetosonic wave instabilities. Using the observed background plasma conditions and assuming near-perpendicular propagation, we have estimated the trapping region of magnetosonic waves in the Earth's plasmasphere.

Our analysis on the magnetosonic wave and proton ring event on 4 December 2012 has demonstrated that the magnetosonic waves are locally excited near the equatorial plasmapause, subsequently propagate inward to lower L shells, and then become trapped over a limited radial region in the outer plasmasphere. This scenario is consistent with magnetosonic wave local excitation mechanism and perpendicular propagation properties in the previous studies [Chen *et al.*, 2010; Chen and Thorne, 2012; Ma *et al.*, 2014]. A similar analysis of the magnetosonic wave event on 6 November 2012 has shown that magnetosonic waves can be excited and trapped in a localized region with enhanced density and can therefore be modulated by density structures in the plasmasphere. However, magnetosonic waves observed deep inside the plasmapause may originate from a source region at very different magnetic local time, which was not sampled along the satellite orbit.

Our proposed trapping mechanism provides a reasonable explanation for most observations of magnetosonic waves in the plasmasphere. The reconstruction of the observed wave power spectrogram

requires a ray tracing technique [e.g., *Xiao et al.*, 2012] and incorporation of the local wave excitation, damping and the propagation effects, which are beyond the scope of this study. Nevertheless, our study clearly demonstrates that the propagation and subsequent trapping in the outer plasmasphere are important to account for magnetosonic wave observations in the plasmasphere.

Acknowledgments

This work was supported by NASA grant NNX11AR64G and by JHU/APL contracts 967399 and 921647 under NASA's prime contract NAS5-01072 and NSF grants AGS 1405041 and 1405054. The analysis at UCLA was supported by the EMFISIS subaward 1001057397:01 and by the ECT subaward 13-041. In this paper, the EMFISIS data are available from <http://emfisis.physics.uiowa.edu/Flight/RBSP-A>, and the ECT HOPE data are available from http://www.rbsp-ect.lanl.gov/data_pub/rbspa/hope. We thank the World Data Center for Geomagnetism, Kyoto, for providing AE indices used in this study.

The Editor thanks Scott Boardsen and an anonymous reviewer for their assistance in evaluating this paper.

References

- Boardsen, S. A., D. L. Gallagher, D. A. Gurnett, W. K. Peterson, and J. L. Green (1992), Funnel-shaped, low-frequency equatorial waves, *J. Geophys. Res.*, 97, 14,967–14,976, doi:10.1029/92JA00827.
- Bortnik, J., and R. M. Thorne (2010), Transit time scattering of energetic electrons due to equatorially confined magnetosonic waves, *J. Geophys. Res.*, 115, A07213, doi:10.1029/2010JA015283.
- Chen, L., and R. M. Thorne (2012), Perpendicular propagation of magnetosonic waves, *Geophys. Res. Lett.*, 39, L14102, doi:10.1029/2012GL052485.
- Chen, L., R. M. Thorne, V. K. Jordanova, and R. B. Horne (2010), Global simulation of magnetosonic wave instability in the storm time magnetosphere, *J. Geophys. Res.*, 115, A11222, doi:10.1029/2010JA015707.
- Chen, L., R. M. Thorne, V. K. Jordanova, M. F. Thomsen, and R. B. Horne (2011), Magnetosonic wave instability analysis for proton ring distributions observed by the LANL magnetospheric plasma analyzer, *J. Geophys. Res.*, 116, A03223, doi:10.1029/2010JA016068.
- Funsten, H. O., et al. (2013), Helium, Oxygen, Proton, and Electron (HOPE) mass spectrometer for the radiation belt storm probes mission, *Space Sci. Rev.*, doi:10.1007/s11214-013-9968-7.
- Gurnett, D. A. (1976), Plasma wave interactions with energetic ions near the magnetic equator, *J. Geophys. Res.*, 81, 2765–2770, doi:10.1029/JA081i016p02765.
- Horne, R. B., G. V. Wheeler, and H. S. C. K. Alleyne (2000), Proton and electron heating by radially propagating fast magnetosonic waves, *J. Geophys. Res.*, 105(A12), 27,597–27,610, doi:10.1029/2000JA000018.
- Horne, R. B., R. M. Thorne, S. A. Glauert, N. P. Meredith, D. Pokhotelov, and O. Santolik (2007), Electron acceleration in the Van Allen radiation belts by fast magnetosonic waves, *Geophys. Res. Lett.*, 34, S09S03, doi:10.1029/L17107.
- Kletzing, C. A., et al. (2013), The Electric and Magnetic Field Instrument Suit and Integrated Science (EMFISIS) on RBSP, *Space Sci. Rev.*, doi:10.1007/s11214-013-9993-6.
- Laakso, H., H. Junginger, A. Roux, R. Schmidt, and C. de Villedary (1990), Magnetosonic waves above $f_c(H^+)$ at geostationary orbits: GEOS 2 results, *J. Geophys. Res.*, 95(A7), 10,609–10,621, doi:10.1029/JA095iA07p10609.
- Liu, K., S. P. Gary, and D. Winske (2011), Excitation of magnetosonic waves in the terrestrial magnetosphere: Particle-in-cell simulations, *J. Geophys. Res.*, 116, A07212, doi:10.1029/2010JA016372.
- Ma, Q., W. Li, R. M. Thorne, and V. Angelopoulos (2013), Global distribution of equatorial magnetosonic waves observed by THEMIS, *Geophys. Res. Lett.*, 40, 1895–1901, doi:10.1002/gra.50434.
- Ma, Q., W. Li, L. Chen, R. M. Thorne, and V. Angelopoulos (2014), Magnetosonic wave excitation by ion ring distribution in the Earth's inner magnetosphere, *J. Geophys. Res. Space Physics*, 119, 844–852, doi:10.1002/2013JA019591.
- Mauk, B. H., N. J. Fox, S. G. Kanekal, R. L. Kessel, D. G. Sibeck, and A. Ukhorskiy (2012), Science objectives and rationale for the Radiation Belt Storm Probes mission, *Space Sci. Rev.*, 179(1–4), 3–27, doi:10.1007/s11214-012-9908-y.
- Meredith, N., R. B. Horne, and R. R. Anderson (2008), Survey of magnetosonic waves and proton ring distributions in the Earth's inner magnetosphere, *J. Geophys. Res.*, 113, A06213, doi:10.1029/2007JA012975.
- Mourenas, D., A. V. Artemyev, O. V. Agapitov, and V. Krasnoselskikh (2013), Analytical estimates of electron quasi-linear diffusion by fast magnetosonic waves, *J. Geophys. Res. Space Physics*, 118, 3096–3112, doi:10.1002/jgra.50349.
- Perraut, S., A. Roux, P. Robert, and R. Gendrin (1982), A systematic study of ULF waves above FH + from GEOS 1 and 2 measurements and their relationships with proton ring distributions, *J. Geophys. Res.*, 87(A8), 6219–6236, doi:10.1029/JA087iA08p06219.
- Russell, C. T., and R. E. Holzer (1970), OGO 3 observation of ELF noise in the magnetosphere. 2. The nature of the equatorial noise, *J. Geophys. Res.*, 75(4), 755–768, doi:10.1029/JA075i004p00755.
- Santolík, O., J. S. Pickett, and D. A. Gurnett (2002), Spatiotemporal variability and propagation of equatorial noise observed by Cluster, *J. Geophys. Res.*, 107(A12, 1495), doi:10.1029/2001JA009159.
- Santolík, O., M. Parrot, and F. Lefèuvre (2003), Singular value decomposition methods for wave propagation analysis, *Radio Sci.*, 38(1, 1010), doi:10.1029/2000RS002523.
- Santolík, O., F. Nemec, K. Gereova, E. Macusova, Y. de Conchy, and N. Cornilleau-Wehrlin (2004), Systematic analysis of equatorial noise below the lower hybrid frequency, *Ann. Geophys.*, 22, 2587–2595, doi:10.5194/angeo-22-2587-2004.
- Spence, H. E., et al. (2013), Science goals and overview of the energetic particle, composition, and thermal plasma (ECT) Suite on NASA's Radiation Belt Storm Probes (RBSP) mission, *Space Sci. Rev.*, doi:10.1007/s11214-013-0007-5.
- Thomsen, M. F., M. H. Denton, V. K. Jordanova, L. Chen, and R. M. Thorne (2011), Free energy to drive equatorial magnetosonic wave instability at geosynchronous orbit, *J. Geophys. Res.*, 116, A08220, doi:10.1029/2011JA016644.
- Xiao, F., Q. Zhou, Z. He, and L. Tang (2012), Three-dimensional ray tracing of fast magnetosonic waves, *J. Geophys. Res.*, 117, A06208, doi:10.1029/2012JA017589.
- Xiao, F., Q. Zhou, Z. He, C. Yang, Y. He, and L. Tang (2013), Magnetosonic wave instability by proton ring distributions: Simultaneous data and modeling, *J. Geophys. Res. Space Physics*, 118, 4053–4058, doi:10.1002/jgra.50401.
- Xiao, F., Q. Zong, Y. Wang, Z. He, Z. Su, C. Yang, and Q. Zhou (2014), Generation of proton aurora by magnetosonic waves, *Sci. Rep.*, 4, 5190, doi:10.1038/srep05190.